THE JOURNAL OF PHYSICAL CHEMISTRY B

Article

pubs.acs.org/JPCB

Reaction Mechanism and Catalytic Fingerprint of Allantoin Racemase

Christophe Bovigny, Matteo Thomas Degiacomi,[†] Thomas Lemmin, Matteo Dal Peraro, and Marco Stenta*[,‡]

École Polytechnique Fédérale de Lausanne (EPFL), CH-1015 Lausanne, Switzerland

Supporting Information

ABSTRACT: The stereospecific oxidative decomposition of urate into allantoin is the core of purine catabolism in many organisms. The spontaneous decomposition of upstream intermediates and the nonenzymatic racemization of allantoin lead to an accumulation of (*R*)-allantoin, because the enzymes converting allantoin into allantoate are specific for the (*S*) isomer. The enzyme allantoin racemase catalyzes the reversible conversion between the two allantoin enantiomers, thus ensuring the overall efficiency of the catabolic pathway and preventing allantoin accumulation. On the basis of recent crystallographic and biochemical evidence, allantoin racemase has been assigned to the family of cofactor-independent racemases, together with other amino acid racemases. A detailed computational investigation of allantoin racemase has been carried out to complement the available experimental data and to provide atomistic insight into the enzymatic action. Allantoin, the natural substrate of the enzyme, has been investigated at the quantum mechanical level, in order to rationalize its conformational and tautomeric equilibria, playing a key role in protein−ligand recognition and in the following catalytic steps. The reaction mechanism of the enzyme has been elucidated through quantum mechanics/molecular mechanics (QM/MM) calculations. The potential energy surface investigation, carried out at the QM/MM level, revealed a stepwise reaction mechanism. A pair of cysteine residues promotes the stereoinversion of a carbon atom of the ligand without the assistance of cofactors. Electrostatic fingerprint calculations are used to discuss the role of the active site residues in lowering the pK_a of the substrate. The planar unprotonated intermediate is compared with the enolic allantoin tautomer observed in the active site of the crystallized enzyme. Finally, the enzymatic catalysis featured by allantoin racemase (AllR) is compared with that of other enzymes belonging to the same family.

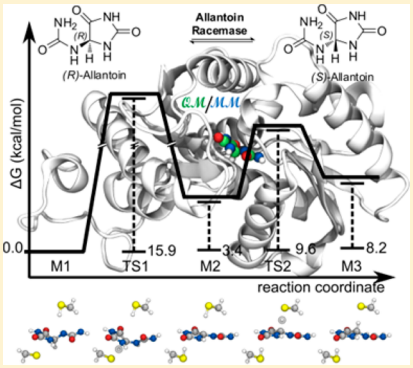

1. INTRODUCTION

Urate, a key intermediate in purine catabolism, is converted into allantoate by the consecutive action of four enzymes (Scheme 1). The stereospecific oxidative decomposition of urate into (*S*)-allantoin[1,2] is initiated by the action of urate oxidase[3] (uricase, EC 1.7.3.3), resulting in the production of 5-hydroxyisourate (HIU). The enzyme HIU hydrolase[4] (EC 3.5.2.17) catalyzes the second step, namely, the conversion of HIU into 2-oxo-4-hydroxy-4-carboxy-5-ureidoimidazoline (OHCU). The following step, leading from OHCU to allantoin, is catalyzed by OHCU decarboxylase[5] (EC 4.1.1.n1). Lastly, the enzyme (*S*)-allantoin amido-hydrolase[6] (allantoinase, EC 3.5.2.5) catalyzes the hydrolytic cleavage of the five-member hydantoin ring, thus yielding the final product, allantoate. The urate catabolic pathway is shared by bacteria, fungi, plants, and animals (including most mammals). Allantoin and its degradation derivatives constitute a source of nitrogen, carbon, and energy for bacteria and play an essential role in the assimilation, metabolism, transport, and storage of nitrogen in plants. On the other hand, the urate catabolic pathway is missing in humans, birds, reptiles, and some bacteria: as a consequence, urate can accumulate in such organisms. In humans, urate can crystallize in joints or in kidneys, thus leading, respectively, to gout or renal stones.

The overall efficiency of urate degradation depends on a fifth enzyme, whose action has remained elusive until recently. While (*S*)-allantoin is the sole product of the stereospecific enzymatic reactions, the spontaneous decomposition of the unstable intermediates HIU and OHCU leads indiscriminately to both (*S*)- and (*R*)-enantiomers. Since all known allantoinases are selective for the (*S*)-enantiomer, a mechanism is required to render (*R*)-allantoin available for enzymatic hydrolysis.

The enzyme allantoin racemase (AllR, EC 5.1.99.3) has been associated with this important function, based on both genetic and structural evidence.[7] In particular, AllR from *Klebsiella pneumoniae* was crystallized, revealing close sequence and structural similarities to hydantoin racemase[8] (HydR, EC 5.1.99.5). On the basis of biochemical evidence, both enzymes have been included in the family of cofactor-independent racemases, since both catalyze racemization of 5-substituted hydantoins without the assistance of any metal or cofactor. Within the family of pyridoxal 5′-phosphate (PLP)-independent racemases, AllR and HydR belong, together with aspartate (AspR, EC 5.1.1.13) and glutamate racemase (GluR, EC

Received: December 1, 2013
Revised: May 17, 2014
Published: June 10, 2014

Scheme 1. Uric Acid Degradation Pathway

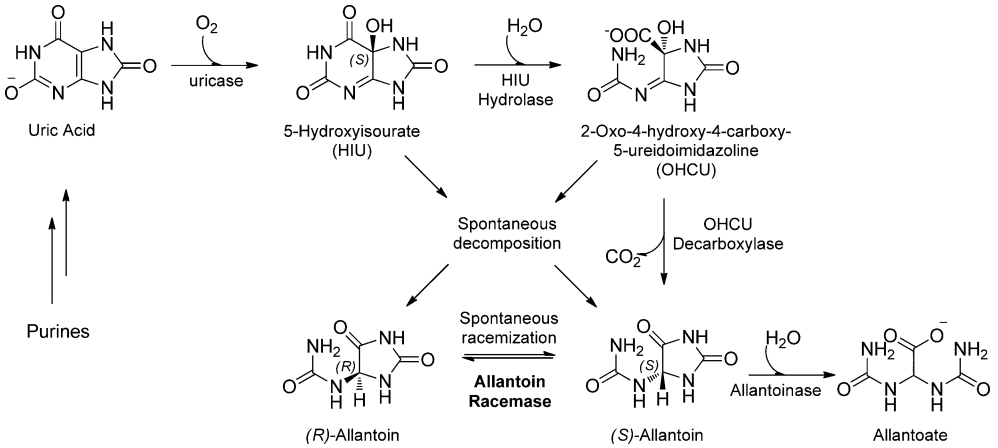

5.1.1.3), to the aspartate transcarbamylase (ATC)-like fold. Other well known racemases, like proline racemase (ProR, EC 5.1.1.4) and diaminopimelate epimerase (DAPE, EC 5.1.1.7), belong to the (DAPE)-like fold.[9]

Racemases put in place remarkable chemical strategies aimed at effectively abstracting the Cα-hydrogen of amino acids, whose pK_a ranges from 21 to 34.[10] In particular, in cofactor-dependent racemases, the substrate is "activated" through the formation of a covalent intermediate with the pyridoxal 5′-phosphate (PLP) moiety, resulting in a drop of the pK_a to sizable values ranging from 6 to 17.[11] In PLP-independent racemases, the catalysis is performed through electrostatic stabilization of the transition state(s),[12] since no covalent intermediate is formed between the substrate and the active-site cysteine residues.

Despite the differences in the overall architecture, all PLP-independent racemases share, in the catalytic site, a couple of cysteine residues involved in both substrate recognition and catalysis. Site-directed mutagenesis, kinetic studies, and iodoacetamide titration support a two-base mechanism involving the two active-site cysteine residues in the form of a thiole/thiolate dyad.[9]

While experimental evidence delineated the global picture of the enzymatic action of PLP-independent racemases, theoretical investigation contributed to a deeper understanding of the atomistic details of both reaction mechanism and catalytic proficiency. The enzymes GluR,[13] AspR,[14] ProR,[15,16] and DAPE[17] catalyze the stereoinversion of the chiral center of their respective substrates by means of a double proton transfer in a highly asynchronous concerted mechanism with a single transition state. In particular, the unprotonated cysteine abstracts a proton from the chiral center of the substrate, while a proton is transferred on the opposite side of same carbon atom by the other cysteine, thus achieving the stereoinversion of the chiral center. GluR constitutes a special case among the investigated cofactor-independent racemases, since the catalytic cysteine couple features neutral thiole moieties instead of a thiole/thiolate dyad. In this case, an aspartate deprotonates one cysteine, thus triggering the mentioned concerted double proton transfer; finally, a histidine residue donates a proton to the nascent deprotonated cysteine. Both Asp and His residues are highly conserved across different species in GluR enzymes, but they are replaced by serine and glycine in AllR and by glycine/serine and glutamate in AspR (see Table S10 and Chart S7 in the Supporting Information). Moreover, in AllR, no residue effectively playing the role performed by the Asp/His couple in GluR is available. For this reason, AllR and, possibly, AspR should feature a reaction mechanism similar to that of the more structurally distant ProR and AspP.[7] On the basis of this working hypothesis, we set up our investigation of the enzyme AllR, as done previously for AspR,[14] ProR,[15,16] and DAPE.[17] We thus started with the reasonable assumption that a thiole/thiolate dyad is present upon formation of the Michaelis complex between AllR and allantoin. As a corollary, we suppose that the initial protonation state of the dyad is restored upon product release through exchange with the solvent, as suggested by deuterium exchange experiments.[18]

Here, we present a series of simulations aimed at understanding the catalytic mechanism of allantoin racemase (AllR). The reaction mechanism is elucidated by characterizing geometrical and electrostatic properties of intermediates and transition states. The interactions occurring along the reaction path between the substrate and enzyme are highlighted, in order to understand the role played by active-site residues in substrate recognition and transition state stabilization. The results obtained from our simulations, combined with the available experimental data, provide the basis for rational design of inhibitors of PLP-independent racemases,[9] a potential target for antibacterial, antifungal, and herbicide compounds. Results are also discussed in the broad context of other PLP-independent racemases, to identify common features and differences in the whole family of enzymes. This information can foster the rational engineering of racemases to be used as tailored catalysts for optically pure unnatural amino acids.[19]

2. COMPUTATIONAL METHODS

Geometry optimizations and frequency calculations on isolated molecules were carried out at the quantum mechanical (QM) level with the Gaussian 09[20] suite of programs at the B3LYP[21−23]/TZVP[24] level, using an implicit solvent description (IEFPCM)[25] to account for the effect of water.

All molecular mechanics (MM) simulations were performed using NAMD 2.8.[26] Analysis of the molecular dynamics (MD) trajectories was performed using the ProDy[27] package. Pictures were then rendered using the VMD[28] software.

The COBRAMM[29] suite of programs was employed to perform quantum mechanical/molecular mechanical (QM/MM) calculations and catalytic fingerprint analysis[15,17] at the QM(B3LYP/TZVP)/MM(*amber-ff99sb*) level.[30] As in

dx.doi.org/10.1021/jp411786z | J. Phys. Chem. B 2014, 118, 7457−7466

ONIOM-like[31] partitioning schemes, a simple "H link atom" approach was used to saturate the dangling bonds resulting from the QM-MM frontier passing through covalent bonds.[32] To remove the spurious degrees of freedom due to the link atom, the orientation of the extra H atom with respect to its QM and MM neighbors was properly constrained during optimization cycles or MD steps. Electrostatics in the system was treated using an "electrostatic embedding" scheme. Hyperpolarization at the QM-MM boundaries featuring a "H link atom" was avoided through a simple charge shift scheme, where the charge of the first MM atom was redistributed on the first-shell neighboring atoms.[32] The fraction of the charge redistributed on each MM atom was kept proportional the original charge; this approach reduced the perturbation of local MM dipoles. To avoid errors in the calculations of long-range interactions, infinite cut-offs were used to describe pure MM and hybrid QM ⇔ MM interactions. Despite its simplicity, this QM/MM scheme is very robust and versatile, as proven by its many successful applications, ranging from PES exploration of enzyme catalysis[15,17,33] to the description of photoinduced dynamics of complex biological systems.[34,35]

Extensive details about the computational method and system setup are reported in the Supporting Information.

3. RESULTS

3.1. Preliminary QM Study on Allantoin. Detailed potential energy surface (PES) investigations were carried out to determine the conformational freedom and the electrostatic properties of allantoin, the substrate of AllR. To understand the enzymatic mechanism of AllR, the enolic tautomer of allantoin and the C8 unprotonated species were compared (Figure 1). In

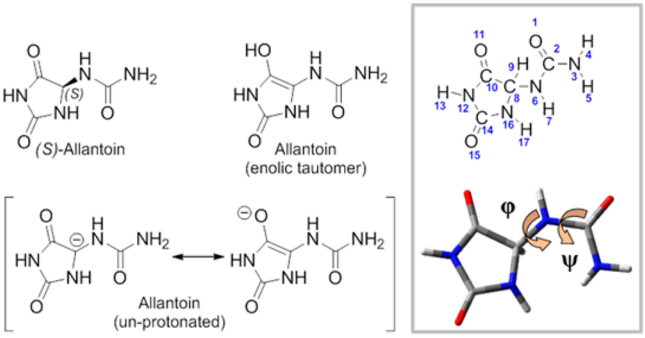

Figure 1. Molecular species investigated at the QM level. The numbering scheme adopted throughout and the dihedral angles discussed in the main text are reported in the inset. The dihedral angles are defined as φ = C10−(C8−N6)−C2 and ψ = C8−(N6−C2)−O1.

fact, while allantoin is the natural substrate of the enzyme, the unprotonated form constitutes a reaction intermediate (see below). Furthermore, the enolic form has been cocrystallized with a mutant of the enzyme, possibly due to its close geometrical resemblance with the unprotonated reaction intermediate.

The linkage between the hydantoin ring and the ureido moiety constitutes the main degree of conformational freedom in allantoin. In addition to this, the ureido moiety itself can switch between the *cis* and *trans* isomers. The conformational space of allantoin and its derivatives can thus be reduced to two dimensions, represented by the two dihedral angles φ and ψ (Figure 1).

In agreement with previous studies,[36,37] the most stable allantoin conformer (T_M1) features a *trans*-ureido isomer. Rotation around the N6−C8 bond leads to the almost isoenergetic (+0.46 kcal/mol) conformer (T_M2); a barrier of about 7 kcal/mol is associated with the rotational transition state. Each of the two minima undergoes isomerization of the ureido moiety through two separate channels, leading to the *cis*-ureido isomers C_M1 and C_M2 (Figure 2). The calculated energy barriers for *trans* → *cis* isomerization range from 11 to 15 kcal/mol. These results suggest that the double bond character of the amide bond is substantially lower in ureido moieties than in other amides,[38] featuring activation energies of up to 30 kcal/mol.[39] This implies that a large fraction of allantoin population features an extended *trans*-ureido group, although the *cis* isomer is expected on the basis of the geometry of the allantoin precursors upstream from the purine degradation pathway (Scheme 1).

The conformational PESs of the other two molecular species considered here (enolic tautomer and unprotonated allantoin, Scheme 1) differ substantially from that of allantoin (Figures S9 and S10 in the Supporting Information). Due to the symmetry plane, the conformational space is halved with respect to that of allantoin, being pairs of minima and transition states related by symmetry. In all of the minima found for either the enolic or the unprotonated allantoin, the ureido moiety is almost perpendicular to the hydantoin ring (φ = 90 ± 10°, see Table S1−S3 in the Supporting Information), whereas the minima in allantoin feature φ angles ranging from 8 to 60°. Another important difference with respect to allantoin lies in the *cis*/*trans* equilibrium of the ureido moiety. For the enolic tautomer, the *cis* isomer C_M1 is slightly more stable (−0.80 kcal/mol) than its *trans* counterpart T_M1. The effect is even more pronounced for the unprotonated allantoin: in this case, the *cis* isomer C_M1 is significantly more stable (−2.95 kcal/mol) than its *trans* counterpart T_M1 (Tables S1−S4 and Figures S1−S4 in the Supporting Information).

Natural bond orbital decomposition (NBO) of the wave function of optimized geometries provides a quantitative support to perturbation molecular orbital (PMO) analysis of the three investigated systems. NBO analysis shows an increasing double bond character of the C8−C10 bond when moving from ketonic to enolic and then to unprotonated allantoin. A perpendicular arrangement of the ureido moiety with respect to the hydantoin ring maximizes the favorable interactions between the bonding π orbital between C8−C10 and the antibonding σ orbitals between C2−N6, N6−H7, and, for *trans* isomers, N3−H5 (respectively $\pi_{CC} \rightarrow \sigma^*_{CH}$, $\pi_{CC} \rightarrow \sigma^*_{NH}$, and $\pi_{CC} \rightarrow \sigma^*_{NH}$); a smaller role is played by the favorable interactions between the bonding σ orbital between H6−H7 and the antibonding π orbital between C8−C10 ($\sigma_{NH} \rightarrow \pi^*_{CC}$) (Scheme 2).

The preference, in the ureido moiety, for the *cis* over the *trans* isomer in enolic and unprotonated allantoin can be explained in terms of 2-orbital-4-electron (steric) repulsion. When the ureido moiety is perpendicular to the hydantoin ring, the *cis* and *trans* isomers expose, respectively, the carbonyl oxygen or the (NH2) amide group to the C8−C10 bond, resulting in a destabilizing interaction that is significantly stronger for the *trans* isomer, due to the lone pair on the oxygen pointing directly toward the C8−C10 bond. For this reason in the unprotonated allantoin, where the C8−C10 bond has an almost full double character, the repulsion between the bonding π orbital and the oxygen lone pair $\pi_{CC}-n_O$ is at its

dx.doi.org/10.1021/jp411786z | J. Phys. Chem. B 2014, 118, 7457−7466

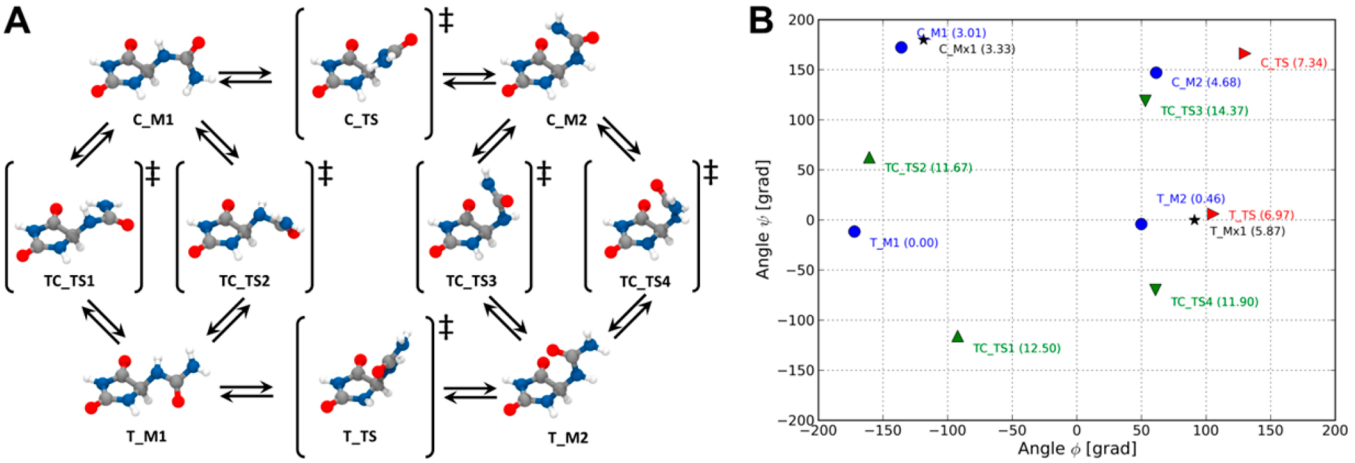

Figure 2. (A) Minima and TS geometries located on the PES of allantoin. Constrained optimization geometries are reported in the insets. (B) Projection of all geometries in the φ, ψ space; energy values (kcal/mol) reported in parentheses refer to T_M1.

Scheme 2. Stabilization of Perpendicular Arrangement via Hyperconjugative Effects (A, B, C); Stabilization of *cis* Isomer for Perpendicular Conformers for Hyperconjugative (C) and Steric (D) Effects

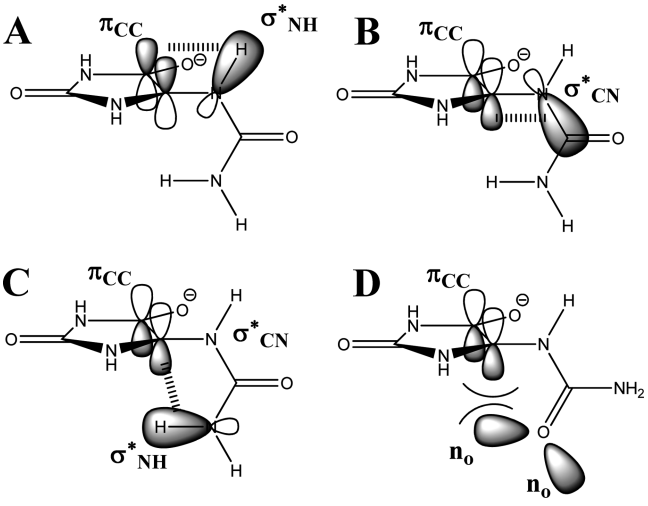

maximum when the arrangement is perpendicular. Nevertheless, the perpendicular arrangement is enforced by the π_{CC} orbital of C8−C10 through the above-mentioned hyperconjugation effects. The two effects result in a destabilization of the *trans* isomer over the *cis* isomer of about 6 kcal/mol, when compared to the ketonic allantoin (+3.1 kcal/mol, favoring the *trans* in ketonic allantoin; −2.95 kcal/mol, favoring the *cis* in unprotonated allantoin). The destabilization is much smaller in the case of enolic allantoin, due to a moderate occupation of the π_{CC} system, resulting in a perpendicular arrangement and in almost energetically equivalent *cis* and *tran* isomers (−0.8 kcal/mol, favoring the *cis*) (Scheme 2).

3.2. QM/MM PES. To build a reliable model of allantoin racemase, we used the crystal structure of the enzyme (*K. pneumoniae* allantoin racemase, Uniprot ID: A6T9E8) in complex with the enolic form of allantoin (PDB ID: 3QVK, resolution 2.00 Å).[7] The cocrystallized substrate was replaced by (*S*)-allantoin. A minimal QM/MM model system (MOD1) was constructed by partitioning the full system into different layers, according to a standard procedure.[15,29] The substrate and the side chains of Cys79 and Cys184 were assigned to the *H* layer, described at the QM level. A number of residues surrounding the *H* layer was included in the *M* layer and optimized consistently with the *H* layer. All of the details of the QM/MM setup are fully reported in the Supporting Information, together with the optimized geometries. The model building, the partitioning scheme, and the optimization protocols closely match those adopted in the study of related enzymes; thus, we refer to the original papers for full details.[15,17,29]

A detailed QM/MM PES exploration revealed that the stereoinversion of allantoin proceeds through a stepwise mechanism, involving a transient intermediate (Figure 3). The two stable minima M1 and M3 represent the complex between enzyme and, respectively, (*S*)- and (*R*)-allantoin. The catalytic dyad adopts, in the two minima, an opposite protonation state: Cys79 is unprotonated in M1 and thus ready to abstract a proton from (*S*)-allantoin, while in M3 the negative charge lies on the side chain of Cys184. In M2, the substrate is fully unprotonated and the geometry of C8 is clearly trigonal. The two transition states TS1 and TS2 connect the intermediate M2 with, respectively, the two minima M1 and M3, and represent two single proton transfers between the substrate and the cysteine dyad. Frequency calculations on the optimized geometries confirmed the nature of the critical points, while IRC calculations allowed assessing the topological connection between minima and TS. The presence of a concerted mechanism involving a single transition state has been ruled out by extensive PES exploration. The existence of an intermediate along the reaction path constitutes a difference with respect to other cofactor-independent racemases, such as proline racemase and diaminopimelate epimerase, featuring a concerted (but highly asynchronous) double proton transfer.

The energy difference between the two minima (8 kcal/mol favoring M1 over M3, Table 1) shows qualitative agreement with the experimental kinetics, supporting that the complex with (*S*)-isomer is slightly more stable.[7] The proton transfer from the substrate to Cys184 (TS1) constitutes the rate-determining step; the calculated barrier of 15.9 kcal/mol is in good agreement with the experimental value of 14.5 kcal/mol (the isomerization of (*S*)-allantoin occurring with k_{cat} = 184 ± 17 s^{-1}).[7] However, the computed energy difference between M1 and M3 cannot be directly compared to the ratio of $R \rightarrow S$ and $S \rightarrow R$ conversion rates, since the energy difference refers only to the catalytic step of the overall enzymatic process. It is

dx.doi.org/10.1021/jp411786z | J. Phys. Chem. B 2014, 118, 7457−7466

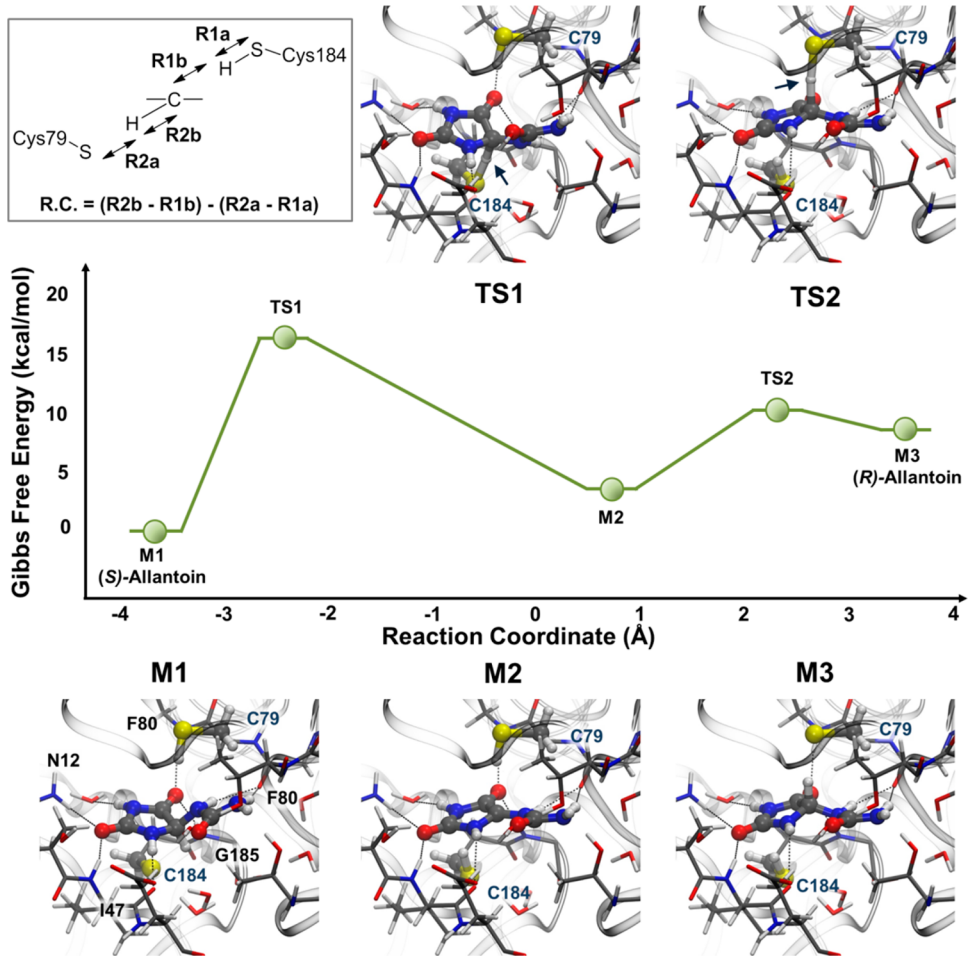

Figure 3. QM/MM reaction profile of allantoin enantiomerization as catalyzed by AllR. The definition of the reaction coordinate is reported in the inset. The geometry of the active site is represented for the critical points found on the PES.

Table 1. Position along the Reaction Coordinate, Energies, and Substrate Geometrical Parameters Calculated for the Critical Points Found on the QM/MM PES[a]

	R.C.	ΔE	ΔG	φ	ψ
M1	−3.7	0.0	0.0	168	−27
TS1	−2.4	20.6	15.9	92	24
M2	0.7	6.3	3.4	163	11
TS2	2.3	12.7	9.6	−177	22
M3	3.5	8.1	8.2	−179	32

[a]Relative electronic and free energies (ΔE and ΔG) are reported in kcal/mol, degrees are used for angles φ and ψ, and the reaction coordinate (R.C.) is reported in Å.

well-known that the key parameters in steady-state kinetics, such as K_M and k_{cat} values, may be functions of rate constants for noncatalytic steps. This is the case for ProR, sharing with AllR the mechanism of action despite the different fold.[40] In this particular case, molecular dynamics simulation of the product (see below), starting from the QM/MM optimized geometry, showed large active site rearrangements, involving several neighboring loops.

Gibbs free energy values are estimated by correction of the internal energy for the thermal contributions, obtained through frequency calculations on the optimized critical points. The energy barriers thus calculated represent a substantial improvement over the uncorrected barrier, as observed in other related cases.[15,17] Free energy simulation would provide energy barriers directly comparable with experimental observables such as binding and kinetic constants. However, this comes at a cost, and often QM/MM free energy simulations rely on the semiempirical method,[13,14] or on reference potentials based on *ad hoc* parametrization. The good qualitative agreement with experimental data suggests that, in this case, a static description of the reaction, based on high level QM/MM geometry optimizations, is able to catch the most important aspects of the enzymatic catalysis.

3.3. Geometrical and Electrostatic Details of Enzymatic Catalysis. To understand enzymatic catalysis and disentangle electrostatic and other geometrical effects, a series of analyses was performed on the stationary points located on the QM/MM PES.

The geometry of the substrate obtained from QM/MM calculations is remarkably different from the one observed in the X-ray structure. In both conformers of the cocrystallized enolic allantoin, the ureido group is almost perpendicular to the hydantoin moiety, thus reflecting the natural preference of the molecule in solution (see above). Instead, both QM/MM minima M1 and M3 feature almost planar (*S*)- and (*R*)-allantoin, with φ angles close to 180°. A bidentate interaction between the *trans* ureido group and the backbone of Gly183 replaces, in the QM/MM structure, the interactions between the *cis* or *trans* ureido group and Thr118 and Thr119 observed in the crystal structure. An energy barrier of ∼12 kcal/mol is

dx.doi.org/10.1021/jp411786z | J. Phys. Chem. B 2014, 118, 7457−7466

associated with the rotation of φ for allantoin in solution (see QM investigation above, Figure 2). The enzyme lowers this barrier and stabilizes the planar arrangement through formation of hydrogen bonds. Molecular dynamics simulations conducted at the MM level (see below and the Supporting Information for details about setup and simulations) revealed that the ureido tail rotates in the ns time scale, switching between planar and perpendicular arrangement, even within the active site. As a check, QM/MM optimizations were performed on selected snapshots featuring a perpendicular arrangement of the ureido moiety; all the located minima feature a slightly higher energy than M1, M2, and M3. Moreover, any attempt to perform a proton transfer from minima featuring a perpendicular tail arrangement failed in yielding a reasonably low transition state.

Taken together, these results shed new light on the catalytic strategy adopted by the enzyme. The pocket is flexible enough to accommodate different substrate geometries. Among the small set of possible arrangements (see the substrate PES described above), only geometries featuring φ angles close to 180° are prone to undergo chemical reaction, while other arrangements (perpendicular) are not. To understand why planar arrangements favor proton abstraction more than perpendicular ones, we performed NBO calculations on the two allantoin conformations both in solvent and within the enzyme active site. When allantoin is forced in a planar arrangement (as in M1 and M3), the lone pair on N6 interacts weakly with the vicinal carbonyl, as testified by its pyramidalization (−23°), and it thus is able to interact with the proximal C−H bond; the resulting $n_N \rightarrow \sigma^*_{CH}$ interaction weakens the C8−H9 bond by populating its antibonding orbital. In other words, a planar arrangement of the ureido moiety, easily accessible even in the enzyme active pocket, weakens the C8−H9 bond and favors proton abstraction, accomplished by one of the two ideally placed Cys side chains.

Similar stereoelectronic effects could be used to explain the spontaneous racemization of allantoin in water. However, experimental evidence suggests that the direct proton abstraction is not the preferred uncatalyzed racemization channel for allantoin. In particular, very little exchange of allantoin H9 for deuterium was observed in phosphate-buffered (pH 7.0) D_2O solution.[18] This finding was later confirmed and furthered by Kahn and Tipton.[37] The authors, based on NMR data and computational investigations, suggest that two pathways are active for allantoin racemization. The major pathway passes through a symmetric bicyclic intermediate, formed by nucleophilic attack of N3 on the C10═O11 carbonyl group; the collapse of such an intermediate leads arbitrarily toward (*S*)- or (*R*)-allantoin. Suggested long ago,[41] this symmetric bicyclic intermediate explains the C2−C14 scrambling observed in the product of urate oxidase,[37] previously (erroneously) attributed to an hypothetical symmetrical intermediate of the urate oxidase catalysis.[42] The main allantoin racemization pathway is, thus, an intramolecular rearrangement and, as a consequence, does not involve proton exchange with the solvent. However, a second, minor racemization pathway based either on a S_E1 or on a S_E2 (back) mechanism is active at higher pH values.[37] Either mechanism can account for the very small proton exchange observed at pH 7.0.[18] A very strong dependency on pH has been observed also for the main racemization pathway: a basic environment would favor deprotonation of (*S*)- or (*R*)-allantoin at the N12 position (pK = 8.4−8.8);[37,43,44] the conformation adopted by the resulting allantoin anion would favor the nucleophilic attack and, thus, the formation of the symmetric bicyclic intermediate.[37] The rate constants for both main and background pathways decrease by a factor of 10 per pH unit below the pK_a of allantoin and, at neutral pH, the half-time of allantoin racemization is greater than 10 h.[37]

As mentioned above, allantoinase catalyzes the production of allantoate with high selectivity toward (*S*)-allantoin. The constant accumulation of the (*R*)-isomer would constitute, in the absence of AllR, a significant physiological bottleneck to purine catabolism. The enzyme AllR increases the racemization rate by 6 orders of magnitude ($k_{cat}/k_{non} = 1.2 \times 10^6$),[7] and as a consequence, the enzyme allantoinase can easily draw off the (*S*)-enantiomer from the pool of racemic allantoin. To ensure a high level of allantoin to allantoate throughput, the catalytic efficiency of AllR should be equal or greater than that of allantoinase. The k_{cat}/K_M value measured for *K. pneumoniae* AllR (6.0×10^5 M^{-1} s^{-1}) is greater than the catalytic proficiency of known allantoinase (700−48 000 M^{-1} s^{-1}).[7]

It is worth remarking that the uncatalyzed and enzymatic racemization pathways feature two completely different mechanisms: while the former passes, via an intramolecualr rearrangement, through a symmetric bicyclic intermediate (hydroxyacetylenediurea), the latter involves acid/base catalysis with exchange of H9 proton with the solvent. The enzyme thus strengthens a pathway resembling the minor uncatalyzed racemization. To this end, the enzyme plays an important role, by providing an optimal scaffold for the catalytic dyad. The two Cys side chains are, in fact, opportunely oriented with respect to the bound substrate to ensure an effective proton shuffle. Although essential, the proper arrangement of the catalytic dyad is, however, not sufficient to ensure deprotonation of C8−H9 by a thiolate moiety, since the weakening effect of the planar arrangement of the ureido moiety does not lower enough the pK_a of the C8 carbon. To this end, the enzyme plays another important role, by actively stabilizing the transition states and the metastable intermediate. In particular, an oxyanion hole stabilizes the negative charge building up on the substrate along the reaction coordinate.[7]

Electrostatic fingerprint analysis of the minima and the transition states (Figure S12 in the Supporting Information) revealed that Gly185 is essential for stabilizing the transition states (TS1 and TS2) and the intermediate (M2) with respect to the minima (M1 and M2). The results obtained by reverse electrostatic fingerprint analysis[17] were then confirmed by QM calculations performed using the MM2QM[45] procedure (Table S5 in the Supporting Information). The H-bond interaction between the N−H of the Gly185 backbone and the carbonyl C10═O11 of the substrate is strengthened in M2 and, to a lesser extent, in TS1 and TS2, owing to the electronic charge accumulating on O11 upon substrate deprotonation. This interaction, responsible for TS stabilization, is also responsible for substrate recognition and in the binding of the allantoin enolic tautomer, also featuring an increased negative charge on atom O11. Peptide backbone mutagenesis, replacing Gly185 with 2-hydoxyacetic acid, could help in assessing the importance of this interaction in TS stabilization and the role of electrostatic stabilization in the catalysis.[12]

The two stable minima M1 and M3, representing the complex between enzyme and, respectively, (*S*)- and (*R*)-allantoin, feature, within the active site, similar hydrogen bond patterns. In both cases, the hydantoin ring is locked in its position by a network of interactions with active site residues. In particular, the side chain of Asn12 and the backbone of Ile47,

dx.doi.org/10.1021/jp411786z | J. Phys. Chem. B 2014, 118, 7457−7466

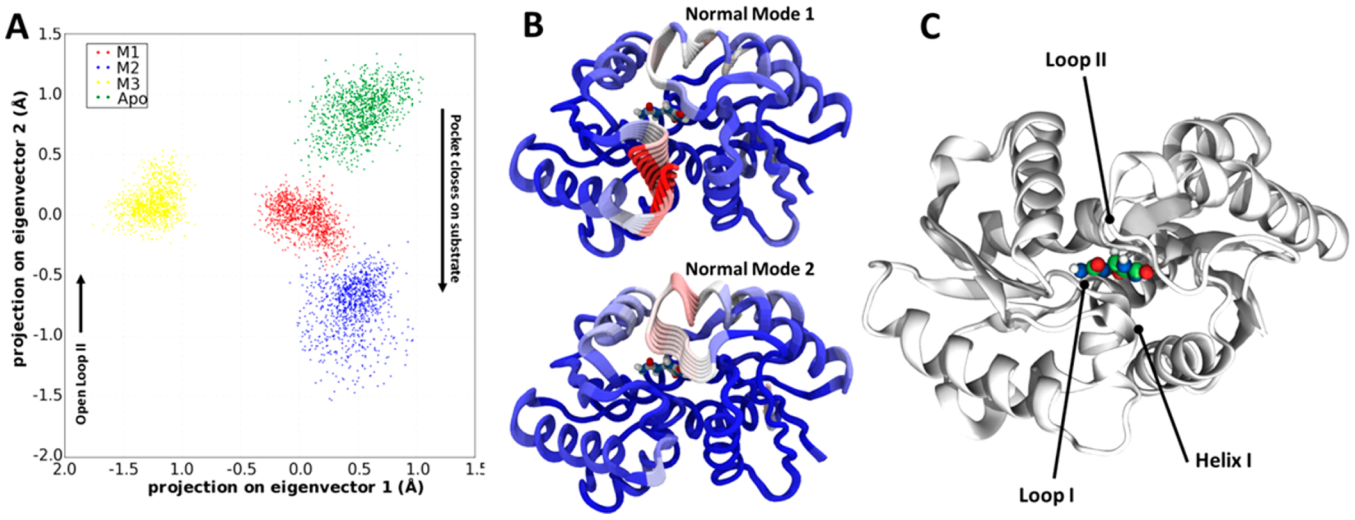

Figure 4. Principal component analysis (PCA) was performed on a set of pooled snapshots from MD simulations of the unligated enzyme (Apo) of M1, M2, and M3 systems: (A) MD trajectories were then projected on the first two principal components. (B) The two first eigenvectors are rendered in tube; red coloring is used for residues predominantly involved in the motion. (C) Cartoon representation of the entire enzyme; the active residue and the catalytic dyad are represented in ball-and-sticks.

Cys79, Phe80, and Gly185 act as H-bond donors; the backbone carbonyl of Ile47 provides a further stabilization by acting as a hydrogen bond acceptor. The ureido moiety of (*S*)-allantoin is kept almost coplanar to the hydantoin ring (φ = 168°) by strong hydrogen bonds with the backbone carbonyl of Gly183. The change of the absolute stereochemistry of C8 is accompanied, along the reaction, by variations in the strength of the hydrogen bond network, due to a different orientation of the ureido tail with respect to the hydantoin core. For instance, in M1, the side chain of Cys184 strongly interacts with the lone pair of (*S*)-allantoin N6. When the stereocenter is fully inverted (as in M3) and Cys184 left unprotonated, the thiol moiety of Cys79 does not effectively interact with the lone pair (*R*)-allantoin N6, despite a nitrogen pyramidalization of +24°. The net loss of this hydrogen bond explains the energy difference between M1 and M3. The transfer of a net negative charge from the side chain of Cys79 to that of Cys184 (almost 8 Å away) can also account for the M1/M3 energy difference. The fingerprint analysis of M1 and M3 minima revealed that positively charged residues (Arg and Lys) stabilize M1 if they are closer to Cys79 (unprotonated in M1 and thus bearing a net negative charge), while negatively charged residues (Asp and Glu) favor M1 only if they are closer to Cys184. The overall electrostatic field, caused by the anisotropic distribution of charged residues around the two catalytically competent cysteine residues, slightly favors M1 over M3.

3.4. Dynamical Features of Substrate Binding. The dynamical features of AllR have been investigated by performing extensive molecular dynamics simulations on the unligated enzyme and on its complexes with (*S*)- and (*R*)-allantoin (M1 and M3) and the unprotonated intermediate (M2). All simulated systems were constructed on the basis of the QM/MM geometries obtained previously; QM/MM charges were employed for the substrate and for the catalytic dyad. Each system was independently equilibrated using the protocol described in the Supporting Information. The analyses were then performed on 100 ns-long equilibrated trajectories.

Principal component analysis on MD trajectories revealed a clear dynamical fingerprint associated with AllR (Figure 4). The first two principal modes are associated with movements of loops I and II and of the α-helix I adjacent to the active site, and account for the opening/closure of the binding pocket. The unligated system, although affected by loop II oscillations, is mostly in an open state. Ligand binding induces a conformational change by modifying the position of loop II with respect to the protein body, as highlighted by the lower values of eigenvector 2 projection of both M1 and M3 MD trajectories. The dynamics of M2, the transient intermediate of the reaction, reveals that the pocket is even more closed, owing to the strong stabilization interactions between protein and substrate discussed above affecting loop II position and flexibility.

M1 and M3, despite an almost identical projection on the eigenvector 2 (position and flexibility of loop II), show a distinct behavior with respect to the eigenvector 1 (position and flexibility of loop I and helix I). The displacement of loop I and helix I allows, after about 70 ns of simulation, for the formation of a channel connecting the active site with the solvent bulk. This channel was not observed in the M1 state, probably due to the tighter binding between (*S*)-allantoin and enzyme (M1). A longer time scale may therefore be required to observe this phenomenon. The mechanism of the substrate access/product egress is currently under investigation by means of accelerated MD techniques, but it is beyond the scope of this article and we leave it therefore to a future scientific report.

4. DISCUSSION

The QM investigation of AllR substrate revealed that allantoin exists as an equilibrium of the two *cis* and *trans* isomers of its ureido moiety. Isomer interconversion takes place through rotation around a particularly weak amide bond (dihedral angle ψ), whose double bond character is substantially lower if compared to standard amide systems.[38] Thus, although the *cis* isomer is expected to be the biologically relevant species (on the basis of the geometry of the allantoin precursors upstream from the purine degradation pathway), the thermodynamically favored *trans* isomer is also present in solution, as a result of the mentioned rapid amide bond isomerization: both *cis* and *trans* isomers have been observed in the crystal structure of the protein−ligand complex.

dx.doi.org/10.1021/jp411786z | J. Phys. Chem. B 2014, 118, 7457−7466

QM/MM geometry optimization of several φ isomers of both *trans* and *cis* allantoin revealed that binding of *trans* allantoin is slightly favored in terms of potential energy, thus confirming that the enzyme is perfectly capable of processing the predominant isomer (*trans*) of its substrate.

The computational investigation presented here suggests a comparison with the geometry of the substrate observed in the X-ray structure. The experimental snapshot of the protein−ligand complex has been achieved by mutating both catalytically competent cysteine residues into a couple of serine residues. The catalytic power of this double mutant is impaired with respect to wild-type enzyme, owing to the fact that the serine couple cannot exert the same acid/base catalysis as the cysteine couple. The much higher pK_a of alcohols with respect to thiols does not allow the formation, even within the active site, of a catalytically competent alcohol/alkoxy dyad. With both serine residues being protonated, the enzyme is unable to bind either (*R*)- or (*S*)-allantoin, but it successfully binds its enolic tautomer, featuring a trigonal C8 atom. A charge distribution analysis on the relevant substrate forms (neutral, unprotonated, enolic) suggests that the same interactions responsible, in the wild-type enzyme, for transition state/intermediate stabilization can contribute, in the crystallized double mutant, to the effective binding of the less stable enolic intermediate.

On the basis of the QM/MM PES, the enolic allantoin observed in the double mutant X-ray structure mimics the unprotonated intermediate occurring along the reaction pathway of the wild-type enzyme. In the M2 critical point, both cysteine residues can, as a matter of fact, be considered fully protonated, with a net negative charge residing on the planar substrate and delocalized in an extended conjugate system.

A major difference between X-ray and the structures obtained by our QM/MM calculations lies in the orientation of the ureido moiety with respect to the hydantoin ring: while in the former the arrangement is almost perpendicular (as observed in the computed minima of solvated allantoin, see Figure S11 in the Supporting Information), in the latter the φ angle accounts for an almost planar arrangement. This apparent discrepancy can be explained on the basis of the reported QM optimizations and MM-MD simulations. The QM PES scan showed that rotation around both the ψ and φ angles involves relatively small energy barriers (below 13 kcal/mol), which is compatible with an exploration of the whole conformational space.

MM-MD simulations revealed that allantoin undergoes a series of conformational changes also within the enzyme active site, capable of accommodating both planar and perpendicular arrangements of the ureido moiety. Upon binding, the substrate undergoes a series of conformational changes in the ureido moiety, while the hydantoin ring is kept fixed at the back of the pocket. Only when the arrangement is almost planar does the first hydrogen transfer to the unprotonated cysteine take place: in this arrangement, the C−H bond is probably further weakened by the $n_N \rightarrow \sigma^*_{CH}$ interaction with the adjacent nitrogen atom. The proton abstraction leaves an unprotonated intermediate, stabilized by conjugation with the rest of the hydantoin ring (mainly the adjacent carbonyl, as highlighted by NBO calculations).

Other members of the same enzyme family catalyze the same stereoinversion reaction but feature a highly asynchronous concerted double proton transfer, with the unprotonated intermediate being a transition state, rather than a minimum. The particular conformational space of unprotonated allantoin, strongly influenced by an intramolecular hydrogen bond, could be taken as a possible reason to explain the difference in the mechanism between AllR and the other enzymes: proline and DAP, the substrates of, respectively, ProR and DAPE, feature no similar intramolecular stabilizing interactions in the unprotonated intermediate.

5. CONCLUSIONS

A detailed investigation of the enzyme allantoin racemase has been carried out to understand its catalytic features. The reaction mechanism, elucidated through QM/MM PES exploration, highlighted some interesting peculiarities, making AllR a one-of-a-kind specimen within the cofactor-independent racemase families. The presence of a stable intermediate along the AllR-catalyzed substrate stereoinversion has been compared to the asynchronous concerted mechanism featured by proline racemase and DAP epimerase.

The substrate of the enzyme, allantoin, has been fully investigated at the QM level in order to understand its structural and electrostatic features, and to allow a fair comparison with the structures obtained at the QM/MM level.

The performed calculations completed the information available through X-ray structure. In particular, the nature of the cocrystallized ligand has been elucidated and related to that of the complex between natural substrate and catalytically competent wild-type enzyme. The analysis of the QM/MM PES revealed that TS stabilization is mainly achieved through an electrostatic stabilization of the transition state.

In addition to that, the dynamics of the system, investigated through molecular dynamics simulations, provided a reasonable hypothesis for substrate access to the binding pocket and for product release following the reaction completion.

The potential energy surface provided, for other enzymes of the family, a fairly accurate approximation of the overall shape of the free energy surface; thus, simple geometry optimizations allowed a good description of the enzymatic catalysis.[15,16] In this case, the energy barriers calculated on the basis of optimized geometries are in good qualitative agreement with the experimental data. We also believe that a dynamical treatment of the reaction mechanism could, in this case, provide further insight on the enzyme functioning.

With this investigation being beyond the scope of the current work, we provide, in the Supporting Information, the relevant geometries of the critical points found, to be used as a starting point for other investigations, such as QM/MM-MD calculations or docking studies.

■ ASSOCIATED CONTENT

Ⓢ Supporting Information

Discussed geometries of allantoin in its neutral, unprotonated, and enolic states are reported in text format, together with energy tables and pictures mentioned in the main text. Extensive details about computational methods and system setup are also provided. The geometries of QM/MM optimized critical points are provided in PDB format in a separate compressed file. The full citation of the Gaussian 09 software is reported. This material is available free of charge via the Internet at http://pubs.acs.org.

■ AUTHOR INFORMATION

Corresponding Author

*E-mail: marco.stenta@gmail.com. Phone: +41628660199.

Present Addresses

†(M.T.D.) Department of Chemistry, University of Oxford, South Parks Road, Oxford, OX1 5QY, U.K.

‡(M.S.) Syngenta Crop Protection AG, Research Chemistry, Schaffhauserstrasse 101, CH-4332 Stein, Switzerland.

Author Contributions

The manuscript was written through contributions of all authors. All authors have given approval to the final version of the manuscript.

Notes

The authors declare no competing financial interest.

■ ACKNOWLEDGMENTS

This work was supported by the Swiss National Science Foundation.

■ ABBREVIATIONS

HIU, 5-hydroxyisourate; OHCU, 2-oxo-4-hydroxy-4-carboxy-5-ureidoimidazoline; AllR, allantoin racemase; HydR, hydantoin racemase; AspR, aspartate racemase; GluR, glutamate racemase; ProR, proline racemase; DAPE, diaminopimelate epimerase; PLP, pyridoxal-5′-phosphate; NBO, natural bond orbital; PMO, perturbation molecular orbital; PES, potential energy surface; TS, transition state; Min, energy minimum; ZPE, zero-point energy

■ REFERENCES

(1) Tipton, P. A. Urate to Allantoin, Specifically (S)-Allantoin. *Nat. Chem. Biol.* **2006**, *2*, 124−125.

(2) Ramazzina, I.; Folli, C.; Secchi, A.; Berni, R.; Percudani, R. Completing the Uric Acid Degradation Pathway through Phylogenetic Comparison of Whole Genomes. *Nat. Chem. Biol.* **2006**, *2*, 144−148.

(3) Retailleau, P.; Colloc'h, N.; Vivares, D.; Bonnete, F.; Castro, B.; El Hajji, M.; Mornon, J.-P.; Monard, G.; Prange, T. Complexed and Ligand-Free High-Resolution Structures of Urate Oxidase (Uox) from Aspergillus Flavus: A Reassignment of the Active-Site Binding Mode. *Acta Crystallogr., Sect. D* **2004**, *60*, 453−462.

(4) French, J. B.; Ealick, S. E. Structural and Kinetic Insights into the Mechanism of 5-Hydroxyisourate Hydrolase from Klebsiella Pneumoniae. *Acta Crystallogr., Sect. D* **2011**, *67*, 671−677.

(5) French, J. B.; Ealick, S. E. Structural and Mechanistic Studies on Klebsiella Pneumoniae 2-Oxo-4-Hydroxy-4-Carboxy-5-Ureidoimidazoline Decarboxylase. *J. Biol. Chem.* **2010**, *285*, 35446−35454.

(6) Kim, K.; Kim, M.-I.; Chung, J.; Ahn, J.-H.; Rhee, S. Crystal Structure of Metal-Dependent Allantoinase from Escherichia Coli. *J. Mol. Biol.* **2009**, *387*, 1067−1074.

(7) French, J. B.; Neau, D. B.; Ealick, S. E. Characterization of the Structure and Function of Klebsiella Pneumoniae Allantoin Racemase. *J. Mol. Biol.* **2011**, *410*, 447−460.

(8) Martinez-Rodriguez, S.; Gonzalez-Ramirez, L. A.; Clemente-Jimenez, J. M.; Rodriguez-Vico, F.; Las Heras-Vazquez, F. J.; Gavira, J. A.; Garcia-Ruiz, J. M. Crystallization and Preliminary Crystallographic Studies of an Active-Site Mutant Hydantoin Racemase from Sinorhizobium Meliloti Cect4114. *Acta Crystallogr., Sect. F* **2008**, *64*, 50−53.

(9) Conti, P.; Tamborini, L.; Pinto, A.; Blondel, A.; Minoprio, P.; Mozzarelli, A.; De Micheli, C. Drug Discovery Targeting Amino Acid Racemases. *Chem. Rev.* **2011**, *111*, 6919−6946.

(10) Tanner, M. E. Understanding Nature's Strategies for Enzyme-Catalyzed Racemization and Epimerization. *Acc. Chem. Res.* **2002**, *35*, 237−246.

(11) Toth, K.; Richard, J. P. Covalent Catalysis by Pyridoxal: Evaluation of the Effect of the Cofactor on the Carbon Acidity of Glycine. *J. Am. Chem. Soc.* **2007**, *129*, 3013−3021.

(12) Warshel, A.; Sharma, P. K.; Kato, M.; Xiang, Y.; Liu, H.; Olsson, M. H. M. Electrostatic Basis for Enzyme Catalysis. *Chem. Rev.* **2006**, *106*, 3210−3235.

(13) Mixcoha, E.; Garcia-Viloca, M.; Lluch, J. M.; González-Lafont, À. Theoretical Analysis of the Catalytic Mechanism of Helicobacter Pylori Glutamate Racemase. *J. Phys. Chem. B* **2012**, *116*, 12406−12414.

(14) Zhang, C.; Guo, Y.; Xue, Y. Qm/Mm Study on Catalytic Mechanism of Aspartate Racemase from *Pyrococcus Horikoshii* Ot3. *Theor. Chem. Acc.* **2011**, *129*, 781−791.

(15) Stenta, M.; Calvaresi, M.; Altoè, P.; Spinelli, D.; Garavelli, M.; Bottoni, A. The Catalytic Activity of Proline Racemase: A Quantum Mechanical/Molecular Mechanical Study. *J. Phys. Chem. B* **2008**, *112*, 1057−1059.

(16) Rubinstein, A.; Major, D. T. Catalyzing Racemizations in the Absence of a Cofactor: The Reaction Mechanism in Proline Racemase. *J. Am. Chem. Soc.* **2009**, *131*, 8513−8521.

(17) Stenta, M.; Calvaresi, M.; Altoè, P.; Spinelli, D.; Garavelli, M.; Galeazzi, R.; Bottoni, A. Catalytic Mechanism of Diaminopimelate Epimerase: A Qm/Mm Investigation. *J. Chem. Theory Comput.* **2009**, *5*, 1915−1930.

(18) Okumura, I.; Yamamoto, T. Enzymic Racemization of Allantoin. *J. Biochem.* **1978**, *84*, 891−895.

(19) Altenbuchner, J.; Siemann-Herzberg, M.; Syldatk, C. Hydantoinases and Related Enzymes as Biocatalysts for the Synthesis of Unnatural Chiral Amino Acids. *Curr. Opin. Biotechnol.* **2001**, *12*, 559−563.

(20) Frisch, M. J.; Trucks, G. W.; Schlegel, H. B.; Scuseria, G. E.; Robb, M. A.; Cheeseman, J. R.; Scalmani, G.; Barone, V.; Mennucci, B.; Petersson, G. A.; et al. *Gaussian 09*, revision A02; Gaussian, Inc.: Wallingford, CT, 2009.

(21) Becke, A. D. Density-Functional Exchange-Energy Approximation with Correct Asymptotic Behavior. *Phys. Rev. A: At., Mol., Opt. Phys.* **1988**, *38*, 3098−3100.

(22) Lee, C.; Yang, W.; Parr, R. G. Development of the Colle-Salvetti Correlation-Energy Formula into a Functional of the Electron Density. *Phys. Rev. B: Condens. Matter Mater. Phys.* **1988**, *37*, 785−789.

(23) Vosko, S. H.; Wilk, L.; Nusair, M. *Can. J. Phys.* **1980**, *58*, 1200−1211.

(24) Godbout, N.; Salahub, D. R.; Andzelm, J.; Wimmer, E. Optimization of Gaussian-Type Basis-Sets for Local Spin-Density Functional Calculations 0.1. Boron through Neon, Optimization Technique and Validation. *Can. J. Chem.* **1992**, *70*, 560−571.

(25) Cances, E.; Mennucci, B.; Tomasi, J. A New Integral Equation Formalism for the Polarizable Continuum Model: Theoretical Background and Applications to Isotropic and Anisotropic Dielectrics. *J. Chem. Phys.* **1997**, *107*, 3032−3041.

(26) Phillips, J. C.; Braun, R.; Wang, W.; Gumbart, J.; Tajkhorshid, E.; Villa, E.; Chipot, C.; Skeel, R. D.; Kalé, L.; Schulten, K. Scalable Molecular Dynamics with Namd. *J. Comput. Chem.* **2005**, *26*, 1781−1802.

(27) Bakan, A.; Meireles, L. M.; Bahar, I. Prody: Protein Dynamics Inferred from Theory and Experiments. *Bioinformatics* **2011**, *27*, 1575−1577.

(28) Humphrey, W.; Dalke, A.; Schulten, K. Vmd: Visual Molecular Dynamics. *J. Mol. Graphics* **1996**, *14*, 33−38.

(29) Altoè, P.; Stenta, M.; Bottoni, A.; Garavelli, M. A Tunable Qm/Mm Approach to Chemical Reactivity, Structure and Physico-Chemical Properties Prediction. *Theor. Chem. Acc.* **2007**, *118*, 219−240.

(30) Warshel, A.; Levitt, M. Theoretical Studies of Enzymic Reactions: Dielectric, Electrostatic and Steric Stabilization of the Carbonium Ion in the Reaction of Lysozyme. *J. Mol. Biol.* **1976**, *103*, 227−249.

(31) Chung, L. W.; Hirao, H.; Li, X.; Morokuma, K. The Oniom Method: Its Foundation and Applications to Metalloenzymes and Photobiology. *Wiley Interdiscip. Rev.: Comput. Mol. Sci.* **2011**, *2*, 327−350.

(32) Lin, H.; Truhlar, D. G. Qm/Mm: What Have We Learned, Where Are We, and Where Do We Go from Here? *Theor. Chem. Acc.* **2006**, *117*, 185−199.
(33) Calvaresi, M.; Stenta, M.; Garavelli, M.; Altoè, P.; Bottoni, A. Computational Evidence for the Catalytic Mechanism of Human Glutathione S Transferase A3−3. A Qm/Mm Investigation. *ACS Catal.* **2012**, *2*, 280−286.
(34) Polli, D.; Altoe, P.; Weingart, O.; Spillane, K. M.; Manzoni, C.; Brida, D.; Tomasello, G.; Orlandi, G.; Kukura, P.; Mathies, R. A.; et al. Conical Intersection Dynamics of the Primary Photoisomerization Event in Vision. *Nature* **2010**, *467*, 440−443.
(35) Weingart, O.; Altoe, P.; Stenta, M.; Bottoni, A.; Orlandi, G.; Garavelli, M. Product Formation in Rhodopsin by Fast Hydrogen Motions. *Phys. Chem. Chem. Phys.* **2011**, *13*, 3645−3648.
(36) Pipolo, S.; Percudani, R.; Cammi, R. Absolute Stereochemistry and Preferred Conformations of Urate Degradation Intermediates from Computed and Experimental Circular Dichroism Spectra. *Org. Biomol. Chem.* **2011**, *9*, 5149−5155.
(37) Kahn, K.; Tipton, P. A. Kinetics and Mechanism of Allantoin Racemization. *Bioorg. Chem.* **2000**, *28*, 62−72.
(38) Terhorst, J. P.; Jorgensen, W. L. E/Z Energetics for Molecular Modeling and Design. *J. Chem. Theory Comput.* **2010**, *6*, 2762−2769.
(39) Hu, X.; Zhang, W.; Carmichael, I.; Serianni, A. S. Amide Cis−Trans Isomerization in Aqueous Solutions of Methyl N-Formyl-D-Glucosaminides and Methyl N-Acetyl-D-Glucosaminides: Chemical Equilibria and Exchange Kinetics. *J. Am. Chem. Soc.* **2010**, *132*, 4641−4652.
(40) Fisher, L. M.; Albery, W. J.; Knowles, J. R. Energetics of Proline Racemase: Racemization of Unlabeled Proline in the Unsaturated, Saturated, and Oversaturated Regimes. *Biochemistry* **1986**, *25*, 2529−2537.
(41) Titherley, A. W. Cxliv.-the Constitution of Allantoin. *J. Chem. Soc., Trans.* **1913**, *103*, 1336−1338.
(42) Canellakis, E. S.; Cohen, P. P. The End-Products and Intermediates of Uric Acid Oxidation by Uricase. *J. Biol. Chem.* **1955**, *213*, 385−395.
(43) Kahn, K.; Serfozo, P.; Tipton, P. A. Identification of the True Product of the Urate Oxidase Reaction. *J. Am. Chem. Soc.* **1997**, *119*, 5435−5442.
(44) Vogels, G. D.; de Windt, F. E.; Bassie, W. Hydrolysis and Racemization of Allantoin. *Recl. Trav. Chim. Pays-Bas* **1969**, *88*, 940−950.
(45) Nowosielski, M.; Hoffmann, M.; Kuron, A.; Korycka-Machala, M.; Dziadek, J. The Mm2qm Tool for Combining Docking, Molecular Dynamics, Molecular Mechanics, and Quantum Mechanics. *J. Comput. Chem.* **2013**, *34*, 750−756.